Heritage Science

RESEARCH ARTICLE

Uncovering the illegible: multi-analytical approach to reveal paint stratigraphy of corroded signposts from the Auschwitz-Birkenau State Museum

Gunn Pöllnitz[1*] , Manfred Schreiner[1], Wilfried Vetter[1], Bernhard Pichler[2] and Andrzej Jastrzębiowski[3]

Abstract

Object discoveries from the Auschwitz-Birkenau State Museum (PMA-B) in Poland challenge the efforts to preserve paint on corroded steel supports. The objects have been exposed to outdoor weathering conditions and then buried for about 65 years. This caused severe damage, such as corrosion and paint delamination. The fragile condition of such cultural heritage objects makes their preservation difficult and comprehensive studies for paint conservation are lacking. Additionally, a thorough investigation of used materials is needed to put objects produced by forced labour in historical context. In this study, we analysed signposts from the Auschwitz-Birkenau State Museum (Poland) collection to gain information about used materials, the object's genesis as well as damage phenomenology. Literature research suggests that the signposts may be produced within the former German NAZI concentration and extermination camp. Inorganic constituents were identified using elemental analysis, such as X-ray fluorescence (XRF) and scanning electron microscopy coupled to an energy dispersive X-ray spectrometer (SEM–EDS). Organic matter was analysed utilizing vibrational spectroscopic instrumentation Fourier transform infrared spectroscopy (FTIR). Our results include the use of synthetic organic pigments (SOPs) and binders, which were newly emerged paint materials at that time. The study highlights the need for conservators to have detailed understanding of composite materials and demonstrates the need for further investigation concerning painted steel objects.

Keywords: Paint on metallic support, Signpost, Synthetic organic pigments, Cellulose nitrate, Preservation, Cultural heritage, World War II, Auschwitz

Introduction

In the course of project P11-0986 "The signposts of the collection of the Auschwitz Museum—Analysis of conservation strategies for coatings on corroded iron substrates", supported by the Future Fund of the Republic of Austria, five signposts were documented and investigated. Three signposts are part of the Auschwitz-Birkenau State Museum (PMA-B) collection, whereas two were provided to the PMA-B's conservation section by

the Gross-Rosen Museum in Rogoźnica (Poland), for study and conservation reasons.

Here, we present the analysis and discussion of two objects from the PMA-B collection [internal designations PMO-U1 (Fig. 1) and PMO-U2 (Fig. 2)].

The arrow-shaped signposts were found by museum's conservator Andrzej Jastrzębiowski, MA, in the area of the former Auschwitz II—Birkenau camp in 2010. The signposts were excavated from the soil and showed severe damages because they have being buried for over 60 years. According to Dębski [1], signposts functioned to arrange the terrain of the extermination site Auschwitz and served to discipline the inmates. Therefore, the signposts "illustrate the terror system and its executive". Today, they provide information about the

*Correspondence: g.poellnitz@akbild.ac.at
[1] Institute of Science and Technology in Art, Academy of Fine Arts Vienna, Schillerplatz 3, 1010 Vienna, Austria
Full list of author information is available at the end of the article

Pöllnitz *et al. Herit Sci*   (2019) 7:98

Page 2 of 12

Fig. 1 Object with internal designation PMO-U1, the property of Auschwitz-Birkenau State Museum, Poland

Fig. 2 Object with internal designation PMO-U2, the property of Auschwitz-Birkenau State Museum, Poland

security system and the organisational structure of the camp. Thus, completing the written and photographic source material for a comprehensive documentation of the concentration camp Auschwitz. Although it is not completely clear, *who* produced the signposts *where* in the camp, Dębski assumes that most of the signposts were produced in so-called *"Malerei-Kommandos"* (painting commands) within the concentration camp. Starting in 1940, the first of such prisoners working units existed in the concentration camp Auschwitz I. This command was obliged to produce several kinds of warning or prohibition signs. The *"Malerei-Kommando"* consisted of between a dozen to over one hundred inmates who were room painters, varnishers or type artists. Later, two additional painting commands were established in camp Auschwitz II—Birkenau, where the described objects were discovered. However, the Schutzstaffel (SS), who owned and operated the defence contractor *"Deutsche Ausrüstungswerke (DAW)"* (German Equipment Works), exploited prisoners in separate painting commands [2] in the area of the extermination site Auschwitz. According to current knowledge, it is not possible to attribute the investigated objects to one particular painting command.

An original photograph [3], which was taken during the liberation of the camp in January 1945, shows a sign with the same shape as the investigated objects. This photographic testimony leads to the question of whether the nowadays illegible inscription could have been "*Umleitung*" (detour)—lack letters on a white background. Therefore, the investigation of original materials should also provide evidence regarding the unreadable inscription in addition to general information such as used pigments, binders and stratigraphic data. Thus, complementary material analyses help to clarify the historic structure and former utilization of these objects.

Experimental

First, we documented the whole object as well as object details by using photography in visible and raking light, IR photography and UV fluorescence (UVF). Cameras in use were DSLR Nikon D2Xs and Fujifilm IS Pro and filters Hoya HMC super UV for UVF and Peca Products 760 nm and 850 nm for IR photography.

Surface examination using optical microscopy (OM) revealed vast lacunae and delamination phenomena between layers distributed over the whole object as could be seen already in macroscopic images Figs. 1 and 2.

Pöllnitz *et al. Herit Sci*   (2019) 7:98

Page 3 of 12

This damage pattern allowed us to determine the edges of the paint on the one hand and distinguish strategic important areas for micro-sampling on the other. These micro-samples were subtly extracted only in areas where corrosion already led to delamination of paint using scalpels and brushes. To reduce the number of samples, we compared loose material from the storage packing—a volatile corrosion inhibitor (VCI) foil—to the extracted micro-samples of the objects. We analysed four samples from each object PMO-U1 and PMO-U2. In the case of PMO-U1, two samples were taken directly from the object and two were finds. Three samples from object PMO-U2 consisted of loose parts and one was chosen strategically. Some of the samples could be used for multiple analyses.

Cross-sections

Two sample fragments from each object were embedded in polyester resin and cross-sections were prepared for paint layer analysis. Paint samples were embedded in polyester resin, type GT (Kurt Wolf & CO, Austria), between two blocks and wet polished (silicon carbide paper grit up to 4000) until the sample material was reached. Microscopic investigations of cross-sections were performed by reflected light microscopy operated with white light (light source: Halogen HAL 100) and UV light (light source: mercury-vapour lamp HBO 100) using an Axioplan 2 Imaging microscope (Carl Zeiss Microscopy, Germany) with photo attachment using a digital camera Nikon D700 and objectives EC-Epiplan Neofluar 50×/0.8, EC-Epiplan Neofluar 20×/0.5 and Epiplan Neofluar 10×/0.3.

Scanning electron microscopy with energy-dispersive X-ray spectroscopy (SEM–EDS)

In addition to optical microscopy (OM), we performed SEM of the cross-sections. Backscattered electrons (BSE), energy dispersive X-ray microanalysis and secondary electrons (SE) were detected to characterize the cross-section's surface. We used a Philips XL-30 ESEM scanning electron microscope (FEI-Philips, USA) with an energy-dispersive X-ray spectrometer (LINK ISIS 300) for acquiring BSE and SE images and for the determination of the elemental composition at an acceleration voltage of 20 kV. To avoid charging effects, carbon sputtering of cross-sections was done prior to analysis.

Fourier transform infrared spectroscopy (FTIR)

FTIR investigations were performed using a LUMOS® FTIR microscope (Bruker Optics, Germany) fitted with a liquid nitrogen-cooled mercury cadmium telluride (MCT) detector in transmission mode. Tiny amounts of sample material were prepared on a diamond cell (SPECTRA TECH, Shelton, CT, USA) with a syringe needle with a 0.3 mm diameter. We collected 64 scans with a resolution of 4 cm^{-1} for the transmission spectra from 4000 to 450 cm^{-1}. The software "OPUS 7.0" served for data acquisition as well as interpretation. The spectra were evaluated by comparison with different databases including IRUG Spectral Database (Version 2000 [4]), ISTA's own historical collection [5], Hummel Industrial Polymers database [6] and Tate Organic Pigment Archive [7].

X-ray fluorescence analysis (XRF)

For XRF investigation we employed a handheld device named xSORT (SPECTRO Analytical Instruments, Germany), equipped with 40 W silver X-ray tube and silica drift detector (SDD), which has a beam diameter of approximately 8 mm. Spectra evaluation was performed with the software X-LabPro. Measurements were carried out in a so-called "docking station", a shielded and lead-lined box with measuring window. We chose settings to detect elements with $Z < 20$ for determination of impurities and soiling. This mode consisted of two measuring cycles, the first 10 s used an excitation voltage of 40 kV and a current of 5 µA, and the second lasted 30 s with 15 kV and 7 µA. Due to the non-destructive character of this method, results in the elemental composition of the colour layers obtained by SEM–EDS could also be extended to other (non-embedded) samples.
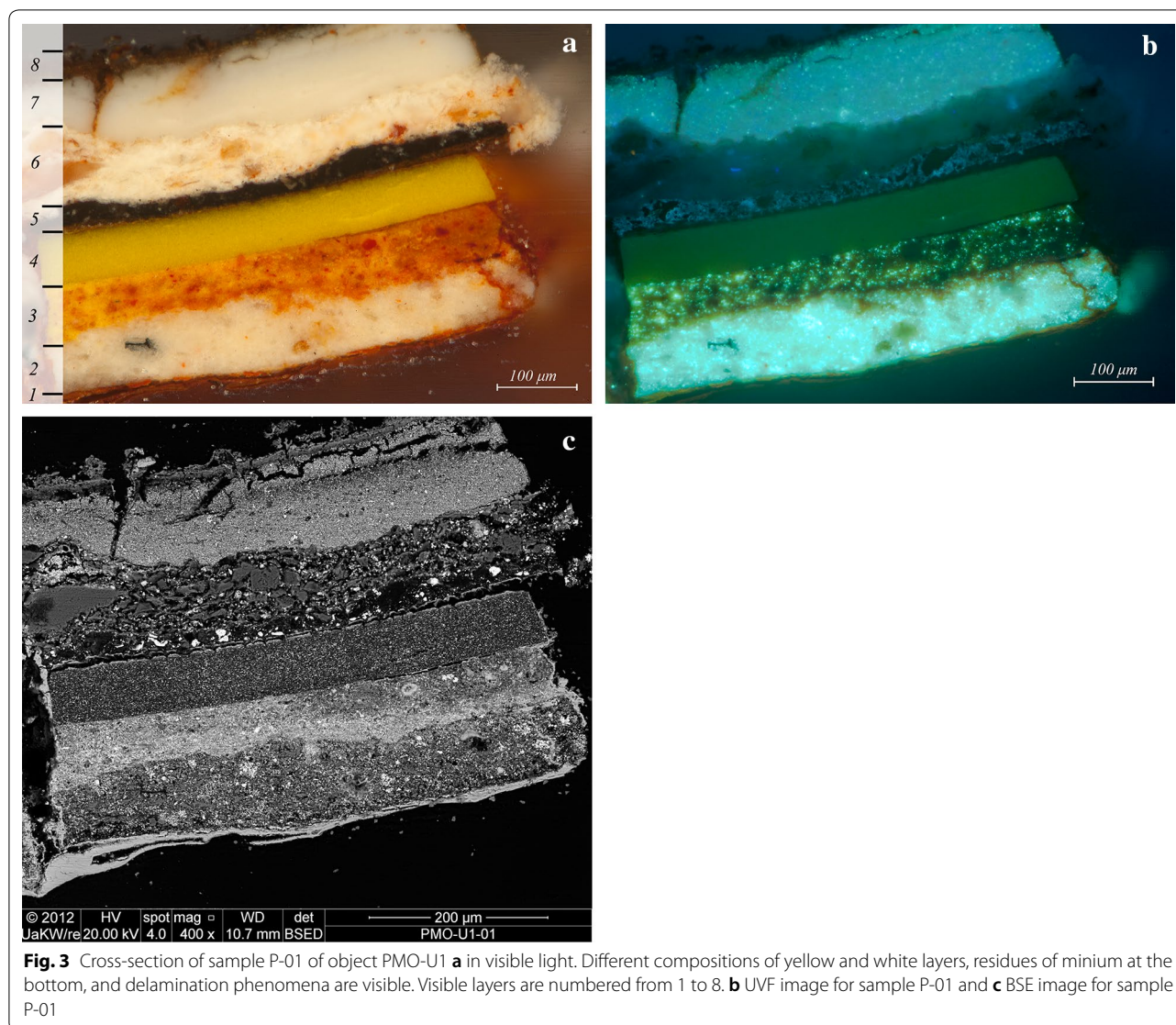
Metallurgical investigations

To obtain more detailed information on the metallic substrates, sample material was examined utilizing etching in order to determine the steel structure. To get information about alloying additions, grain boundaries and microstructure of the substrate, it is necessary to attack the metal's surface with specific chemical reagents [8]. To this end, specimens were embedded in a vacuum with a two-component epoxy resin. The etching of the surfaces of the specimens was carried out through dip etching in 2% Nital (98 ml of methanol and 2 ml of nitric acid, 65% solution in water, 3 s) and wipe etching (30 s) with the same reagent.

Results and discussion

Pigments and binders of PMO-U1

Due to the severe corrosion of the objects, metallurgical investigations could only proof several oxides but no steel structures on the sample surface. By the use of SEM–EDS, we detected the main elements Pb and O in the preparation layer (layer 1 in Fig. 3a–c, Table 1) of object PMO-U1. These results indicate the presence of minium pigment (Pb_3O_4), which was historically used for iron-containing substrates [9, 10]. It is known that minium

Pöllnitz *et al. Herit Sci*   (2019) 7:98

Page 4 of 12

Fig. 3 Cross-section of sample P-01 of object PMO-U1 **a** in visible light. Different compositions of yellow and white layers, residues of minium at the bottom, and delamination phenomena are visible. Visible layers are numbered from 1 to 8. **b** UVF image for sample P-01 and **c** BSE image for sample P-01

yields corrosion protection properties for ferrous metals in combination with oil-based paints due to the formation of different lead soaps. Particularly lead azelate showed to be of high importance [11–13] in this context. According to literature [14], only some lead soaps of linseed oil fatty acids—as azelaic or pelargonic acid—showed to be effective inhibitors. It was also shown that lead salts were more efficient inhibitors than calcium or sodium salts of the same acids [15]. A possible explanation for the inhibitive effect of lead azelate might be the accelerating of oxidation to form ferric salts for reinforcing the metal's oxide film until it's impermeable to ferrous ions [16].

The preparation layer is superimposed by a white layer (layer 2 in Fig. 3, Table 1) which is composed of different pigments. The main elements Zn and Ca argue for a mixture of zinc white (ZnO) and chalk ($CaCO_3$). Traces of Ba and S might be due to barite ($BaSO_4$) and Si could be a hint for soiling of the object, as this element is minorly detected in most of the layers (Table 1).

On top of the white paint two yellow layers could be identified (layers 3 and 4 in Fig. 3). Layer 3 is composed of different pigments as main elements such as O, Cr, Fe, Zn and Pb do indicate a mixture of yellow ochre, chrome yellow ($PbCrO_4$ [17, 18]) and zinc white. Trace elements found by elemental analysis such as Al and Si, suggest the presence of impurity clay minerals in natural earth pigments or residues from polishing.

Layer 4 consists mainly of chrome yellow. FTIR results reveal cellulose nitrate as the binder (Fig. 4a). Nitrate

Pöllnitz *et al. Herit Sci*   (2019) 7:98

Page 5 of 12

Table 1 Overview of examination results of colourants and binders for objects PMO-U1 and PMO-U2

Object	Sequences	FTIR band assignments	SEM/EDS elements	XRF elements	Interpretation
PMO-U1	4th paint sequence White	**L8**:/ **L 6**&**7**: 2928, 2855, 1741, 1579, 141, 1415, 1165, 500	**L8**: O, Al, <u>Si</u>, P, S, (Cl, K, Ca, Ti), Fe, <u>Zn</u> **L 7**: O, (Ca), <u>Zn</u> **L 6**: <u>O</u>, <u>Mg</u>, Al, Si, S, Ba, Ti, (Fe, Zn)	Specimen's upper surface: Si, P, Ca, Ti, (Cr, Mn), <u>Fe</u>, <u>Zn</u>, <u>Pb</u> Specimen's lower surface: (S, Ca, Mn), <u>Fe</u>	Blackish porous soiling layer on top 2 layers: zinc white and barite/titanium white Binder is linseed oil
	3rd paint sequence Black	**L 5**: 2928, 2855, 1738, 1581, 1087, 798, 782, 635, 610	**L 5**: O (Al), Si, S (K), Ca, Ba (Fe, Zn)		Barite and carbon-based black Binder is linseed oil
	2nd paint sequence Yellow	**L 4**: 2962, 2933, 1721, 1654, 1600, 1580, 1380, 1280, 1073, 839, 747, 628, 598	**L 4**: O, <u>Pb</u>,Cr **L 3**: O, (Al, Si, Ca, Ba), Cr, Fe, <u>Zn</u>, <u>Pb</u>		2 layers: chromium yellow and ochre, kaolin, binder is probably blended of cellulose nitrate and alkyd
	1st paint sequence White	/	**L 2**: O, (Al, Si, S), <u>Ca</u>, (Ba, Fe), <u>Zn</u>		Zinc white, barite and chalk
	1st preparation Orange	/	**L 1**: <u>O</u>, (Si, S), <u>Fe</u>, Zn, (Pb)		Rests of minium
	Rests of corrosion	/	/		
PMO-U2	4th paint sequence White	/	**L9**: O, (Mg), <u>Al</u>, <u>Si</u>, (P, K, Ca, Ti, Mn), Fe, (Zn) **L 8**: O, (Mg, Al), Si, <u>Ti</u>, (Fe, Zn) **L7**: O, (Si), <u>Zn</u> **L6**: O, Mg, (Al), <u>Si</u>, S, Ca,, Ba, <u>Ti</u>, (Fe, Zn)	Specimen's upper surface: Si, P, S, (Cl, K), <u>Ca</u>, Ti, (Cr, Mn), Fe, <u>Zn</u> Specimen's lower surface: Si, P, (Cl, K), Ca, Ti,(Mn), Fe, Zn	Blackish porous soiling layer on top 3 layers: zinc white and titanium white
	3rd paint sequence Black	/	**L 5**: O, (Al), <u>Si</u>, S, Ca, Ba, (Fe, Zn)		Barite and carbon-based black Binder is linseed oil
	2nd paint sequence Yellow	**L 4**: 2927, 2856, 2515, 1796, 1731, 1666, 1418, 1294, 1271, 1177, 876, 803, 712	**L 4**: O, Mg, (Al), Si, (S), <u>Ca</u>, (Ba, Fe, Zn)		2 layers: chromium yellow and ochre, barite, chalk and Pigment Yellow 1 (PY1) Binder is linseed oil
	1st paint sequence White	**L 3**: 2927, 2856, 2512, 1796, 1740, 1450, 1189, 1128, 1085, 874, 712, 639, 612, 500	**L 3**: O, (Si), S, Ca, Ba, (Fe), <u>Zn</u>		Mixture of zinc white, barite and chalk
	1st preparation Orange	/	**L 2**: <u>O</u>, Si, (S), <u>Ca</u>, Fe, (Zn)		Chalk and ochre
	Rests of corrosion	/	**L 1**: <u>O</u>, (Si, S, Ca), <u>Fe</u>, (Zn)		Contain partially sulphur

L means layer. Main components detected by elemental analysis are underlined, whereas minor constituents are bracketed

group absorptions are seen in the FTIR spectrum at 1654, 1280, 839 and 747 cm^{-1} [19] as well as a broad band characteristic for C–O acetal in cellulose nitrates at 1073 cm^{-1} [20].

Since its development in 1875 cellulose nitrate or nitrocellulose had numerous applications as explosive, paint, adhesive but also propellant and jewellery due to its low cost and good adhesive properties [21, 22]. Cellulose consists of a large number of anhydroglucose units, six-membered pyranose rings having three hydroxyl (–OH) groups attached to them. Nitric acid can react with those three hydroxyl groups to form nitrate ester. The cellulose nitrate type used for coatings has an average nitrogen content of 12% [23]. During ageing, nitrogen oxides react with water to form nitric acid, which then reacts with iron to form hygroscopic iron (II) and (III) nitrates. Other acids present in the films such as acetic, formic or sulphuric acid also exacerbate iron corrosion [24]. According to literature

cellulose nitrate was blended with other resins to improve properties like gloss, adhesion and hardness [19], in the actual sample, a characteristic doublet for C=C aromatic stretch at 1600 cm^{-1} as well as C=O stretching band at 1721 cm^{-1} could be attributed to alkyd [25, 26] as blending resin. Chrome yellow bands (Fig. 4a), as also identified by SEM–EDS (Table 1), interfere with the binder absorptions in the lower wavenumber region, but a broadening of the bands at 1050 and 860 cm^{-1} due to Cr–O stretching is documented as well as the doublet at 628 and 598 cm^{-1} characteristic for the lead chromate form [18, 19]. Since the beginning of the nineteenth century lead chromate pigments have been produced in yellow, orange and red shades and also have been added to iron oxide pigments as a brightening agent. The major use of this pigment in modern times as road marking paint is mentioned [27].

For the black layer 5 (Fig. 3a–c) a carbon-based black is assumed. The FTIR spectrum (Fig. 4b) does not
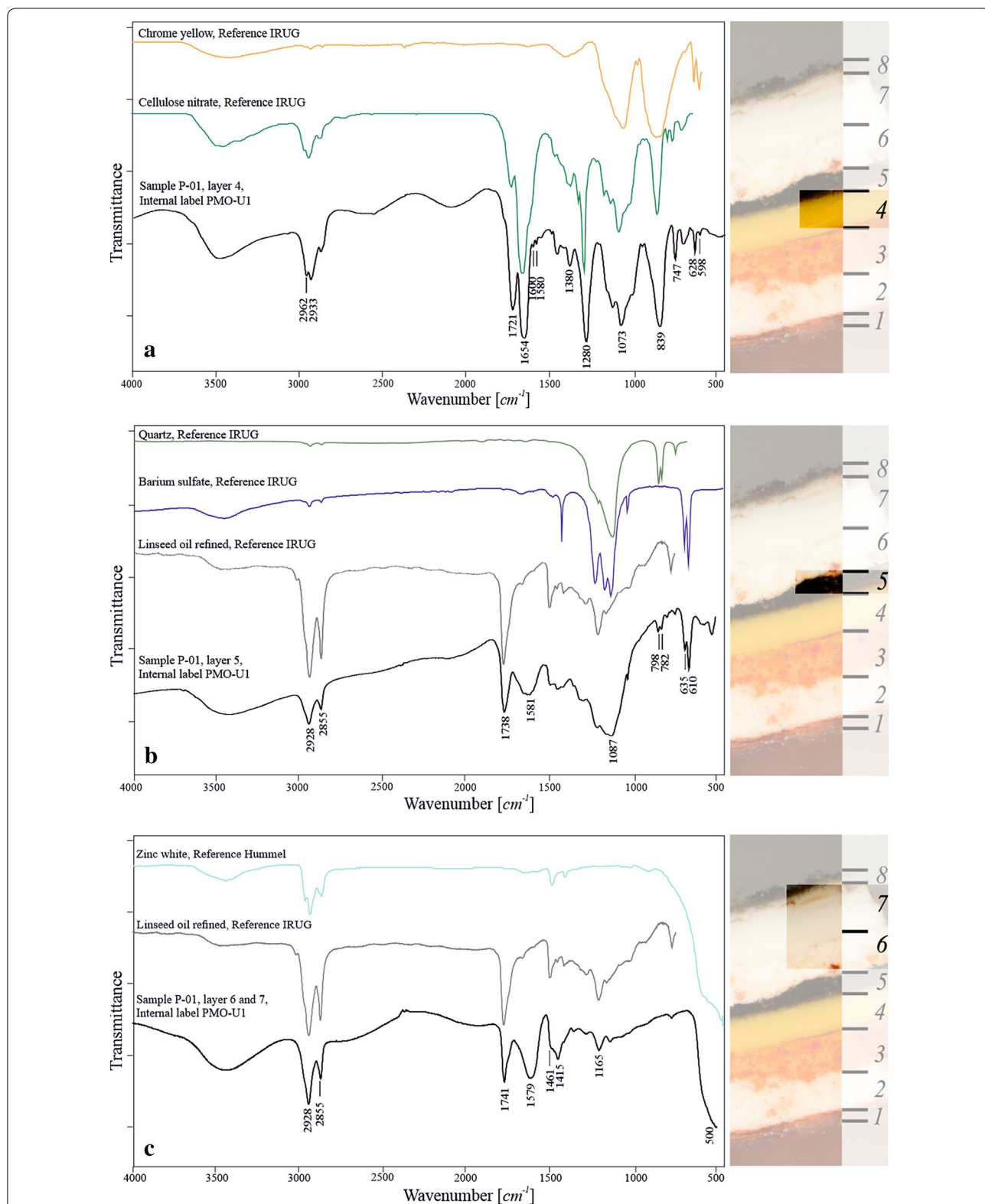
Pöllnitz *et al. Herit Sci*   (2019) 7:98

Page 6 of 12

Fig. 4 Molecular identification of the pigments and binders used for object PMO-U1 **a** the spectrum of yellow layer 4 of sample PMO-U1-01 (black) in comparison with the reference spectra in IRUG database for cellulose nitrate (green) and chrome yellow (yellow). **b** FTIR spectrum of black layer 5 of sample PMO-U1-01 (black) in comparison with the reference spectra in IRUG database for linseed oil (grey), barite (blue) and quartz (dark grey). **c** The spectrum of white layers 6 and 7 of sample PMO-U1-01 (black) in comparison with the reference spectra in IRUG and Hummel databases for linseed oil (grey) and zinc white (cyan)

Pöllnitz *et al. Herit Sci*   (2019) 7:98

Page 7 of 12

provide characteristic bands for other pigmentation used in paint industry, e.g. iron oxide black, a mixture of magnetite and hematite [28], showing broad bands at 470–590 cm^{-1} [29, 30] or bone black with a fingerprint band around 2010 cm^{-1}, which assignment is discussed in literature [31–35]. Some additions of silicates and barite extender could be determined by FTIR. A broad band at 1087 cm^{-1}, the characteristic doublet at 798 and 782 cm^{-1}, as well as a shoulder at 697 cm^{-1} occur due to quartz in the mixture [36, 37]. Asymmetric stretching in the region between 1200 and 1050 cm^{-1} and a doublet at 635 and 610 cm^{-1} due to vibrational bending of S−O are attributed to barite [36].

For the two white layers 6 and 7 different pigmentations were documented. Non UV fluorescing layer 6 (Fig. 3b) showed mainly O, Mg, S, Ba, Ti and Zn in the elemental analysis, which led to the assumption of a mixture of lithopone, titanium white and mineral fillers. SEM–EDS results of UV fluorescing layer 7 revealed O and Zn with traces of Ca on the contrary, which indicates the use of zinc white with impurities of chalk.

The FTIR spectrum (Fig. 4c) of layer 7 shows C-H stretching vibrations in the region 2928 and 2855 cm^{-1} as well as characteristic C=O stretching at 1741 cm^{-1}, shoulders at 1461 cm^{-1} (C–H bending) and 1165 cm^{-1} (C–O stretching) could be attributed to linseed oils [36]. In addition to the results of elemental analysis usage of zinc white could be documented as a strong broad band in 500 cm^{-1} region [38].

On top, also in accordance with the actual surface of the object, there is a blackish porous layer (layer 8 in Fig. 3a, Table 1) with an elemental composition of O, Al, Si, P, S, Cl, Fe and Zn. This is probably due to soiling at the place of discovery. As zinc white proves to be stable in the sense that it does not discolour [39], questions about

reasons for the blackening emerged. An unconfirmed hypothesis might be the formation of black corrosion products of aluminium and zinc as analysed on Al–Zn alloys. In those layers bayerite (Al(OH)$_3$) and basic zinc aluminium carbonate (Zn$_6$Al$_2$(OH)$_{16}$CO$_3$.4H$_2$O) were identified [40].

Pigments and binder of PMO-U2

Using elemental analysis there was no Pb (lead–elemental component of minium) detected in the orange preparation layer 2 (Fig. 5a, b), as it was the case for PMO-U1. SEM–EDS results reveal mainly O, Ca, Si and Fe, which were interpreted as a mixture of ochre and chalk (CaCO$_3$). Micaceous iron oxides (MIO), pigments containing 80–90% of Fe$_2$O$_3$ in a mostly lamellar shape, are known to have good anticorrosive qualities in pigmented coatings on steel structures due to their barrier effect. The effect is caused by parallel orientation of the particles in the dried film as well as a certain UV protection for the organic matter [11, 29, 41]. However, MIO have a metallic, silver-grey appearance according to the crystalline hematite phase and could be excluded as the actual sequence has an orange colour.

Due to SEM–EDS results mainly Ca, S, Ba, Zn and O were detected for white layer 3 and therefore usage of zinc white (ZnO), barite (BaSO$_4$) and chalk (CaCO$_3$) was concluded (Table 1). Complementary use of FTIR (Fig. 6a) revealed C–H stretching vibrations in the region 2927 and 2856 cm^{-1} as well as characteristic C=O stretching at 1740 cm^{-1}, which could be attributed to linseed oils [36]. The occurrence of zinc white could be documented as a strong broad band in the 500 cm^{-1} region [38]. Barite with characteristic bands in the region between 1200 and 1050 cm^{-1} and a doublet at 635 and
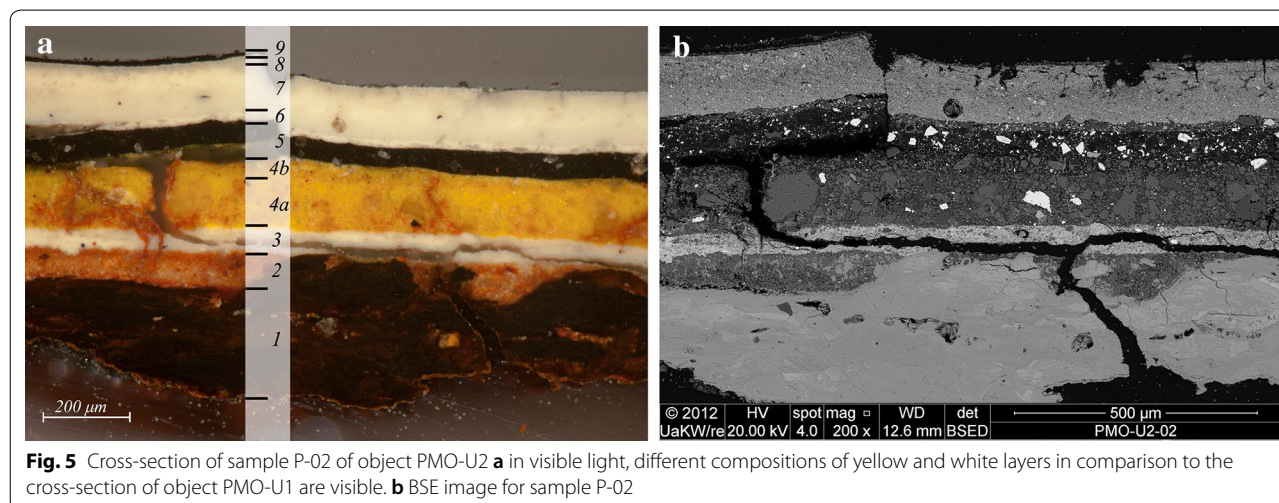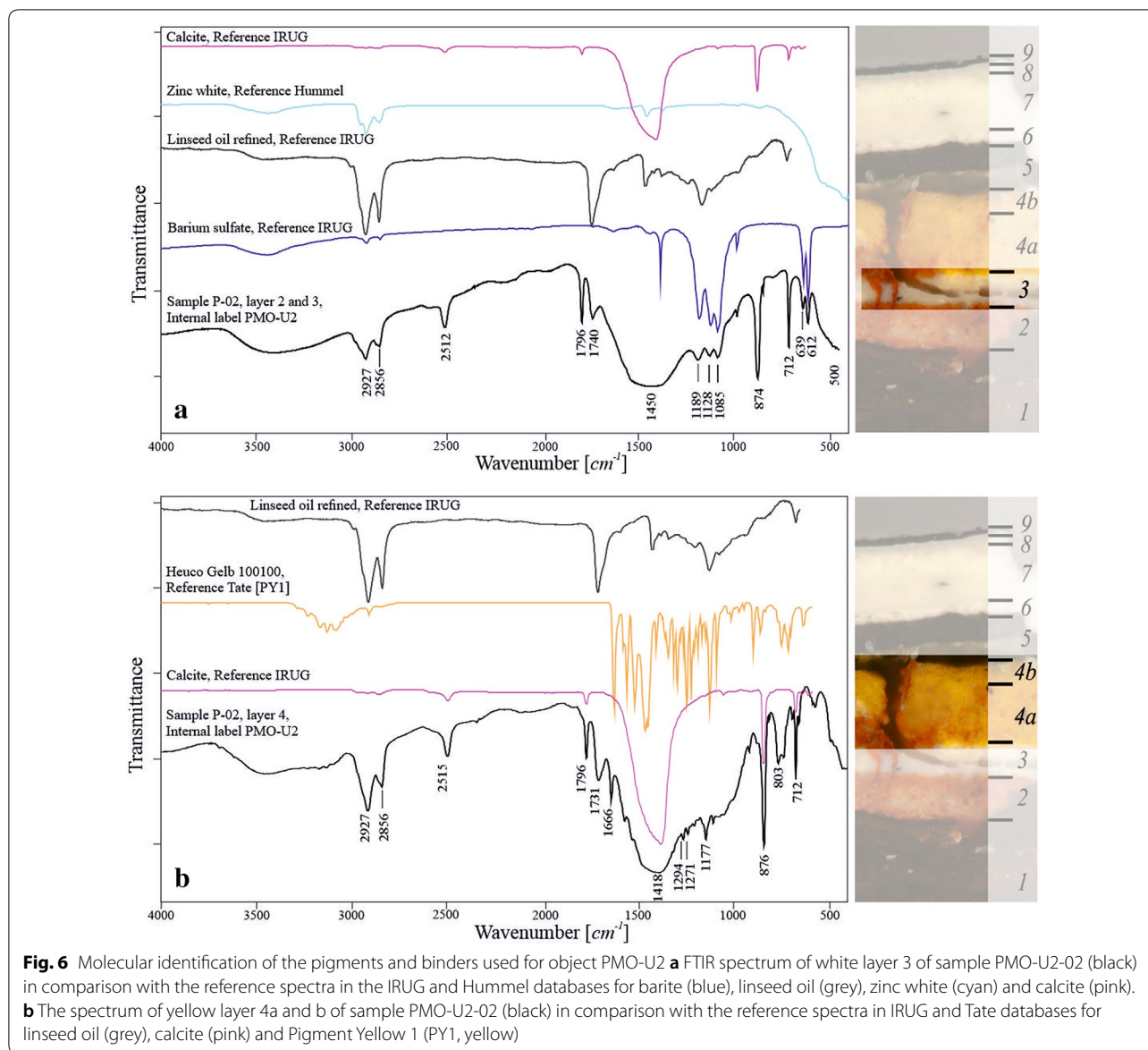

Fig. 5 Cross-section of sample P-02 of object PMO-U2 **a** in visible light, different compositions of yellow and white layers in comparison to the cross-section of object PMO-U1 are visible. **b** BSE image for sample P-02

Pöllnitz *et al. Herit Sci*   (2019) 7:98

Page 8 of 12

Fig. 6 Molecular identification of the pigments and binders used for object PMO-U2 **a** FTIR spectrum of white layer 3 of sample PMO-U2-02 (black) in comparison with the reference spectra in the IRUG and Hummel databases for barite (blue), linseed oil (grey), zinc white (cyan) and calcite (pink). **b** The spectrum of yellow layer 4a and b of sample PMO-U2-02 (black) in comparison with the reference spectra in IRUG and Tate databases for linseed oil (grey), calcite (pink) and Pigment Yellow 1 (PY1, yellow)

610 cm^{-1} as well as calcite with bands at 2512, 1796, 1450 and 874 cm^{-1} are present in the white mixture [36].

The yellow layers 4a and 4b showed differences in the grain size distribution in the cross-section (Fig. 5a), but no composition differences in the SEM–EDS (Fig. 5b). However, their elemental composition differs from those yellow sequences of PMO-U1 and show mainly Ca, Fe, Mg and Si—a mixture of chalk ($CaCO_3$) and ochre (primarily goethite (α–$Fe^{3+}O(OH)$, but also lepidocrocite (γ–$Fe^{3+}O(OH)$ [42]). Additionally, complementary FTIR investigations revealed the occurrence of synthetic azo Pigment Yellow 1 [PY1 [19] (Fig. 6b]. Discovered in 1909, Pigment Yellow 1 is the oldest monoazo (azo group −N=N–) pigment and entered

the market with the name "Hansa Yellow G" [43, 44]. Although monoarylide pigments as e.g. PY1 and PY3 are not easily differentiable by FTIR spectroscopic tools [45], subtle differences were found in better fitting band positions of the sample and the PY1 reference. The spectrum shows a doublet at 1297 and 1271 cm^{-1} which is documented for PY1 [19] and no feature at 1037 cm^{-1} due to aromatic chloro group of PY3, which is the main diagnostic difference according to Lomax et al. [45]. Linseed oil was probably used for yellow layer 4, as characteristic C-H stretching bands at 2927 and 2856 cm^{-1}, as well as a carbonyl band at 1731 cm^{-1} do indicate.

SEM–EDS results for the black layer 5 of sample PMO-U2 reveal mainly O, Si, S, Ca and Ba as also documented for the black layer of PMO-U1 (Table 1). No elemental hint was found for iron-containing blacks or Mn for manganese dioxide black, which led to the conclusion that carbon-based black with barite extender was applied. Investigation with complementary FTIR could not be accomplished due to a lack of sample material.

For the white layer 6 (Fig. 5) SEM–EDS recorded mainly O, Mg, Si, S, Ca, Ba and Ti. A mixture of titanium white with barite and mineral fillers is therefore concluded. Cheap extenders for titanium white, such as $BaSO_4$ and $CaSO_4$, were commonly used [46]. They reduced costs without losses of the extraordinary tinting strength of the more expensive TiO_2. Even more, composite pigments obtained by precipitation of anatase (titanium white) on barium or calcium sulphate were long time considered superior to pure titanium dioxide pigments [47].

Zn and O (Table 1) were identified with elemental analysis in the white layer 7 (Fig. 5), which indicates zinc white. Mainly Ti, but also traces of Zn, Mg and Al, were detected in white layer 8 and hence the use of titanium white is assumed. Traces of zinc in the titanium white could be due to the addition of zinc white for enhancement of drying and permanence as well as reduction of chalking of titanium white, which was common in industrial production [46, 47]. Although discrimination between rutile and anatase form of titanium white could not be achieved with the chosen analytical methods, anatase is estimated, as rutile was not discovered until 1938 [46] and not commercially available until after World War II [48].

Experiments by Carlyle et al. [49] dealing with historically reconstructed grounds for paintings showed that interpretation of stratigraphic layering is challenging. Attention has to be given to the fact that separation of mixtures during drying could occur and would change the appearance of the stratigraphy. In the actual case, three white layers could be present due to separation of materials upon ageing or three single applications of white paint, although no contamination grains are seen in between.

Again a blackish, porous soiling layer seemingly well adheres to the top white paint. SEM–EDS detected mainly O, Al, Si, Fe, Mg and Zn, which in accordance to object PMO-U1 led to the hypothesis of soiling and subsequent corrosion at the place of discovery.

Table 1 gives an overview of the results obtained by FTIR and SEM–EDS on the colourants and binder components of the individual layers of the two objects PMO-U1 and PMO-U2.

UV fluorescence photographs revealed partly yellow-greenish fluorescence (Fig. 7), which could be attributed to the presence of zinc white (ZnO) [50] and was confirmed by SEM–EDS results. No further information about the eventual black inscription on white paint could be generated by the use of IR photography (Fig. 8).

Conclusion

In this study, we analysed two signposts from the PMA-B collection which were found in Auschwitz II—Birkenau. Our results confirm the assumed former white appearance of the objects. However, our analysis did not find a trace of the final black lettering on the uppermost white paint as it was depicted on the historic photograph. We could not conclusively establish the purpose of the black paint sequence, which lies between the upper white and the yellow paint layer. Our results show that both objects were not only painted continuously white but also had yellow sequences. The findings lead to further questions concerning possible reutilization of the substrate.
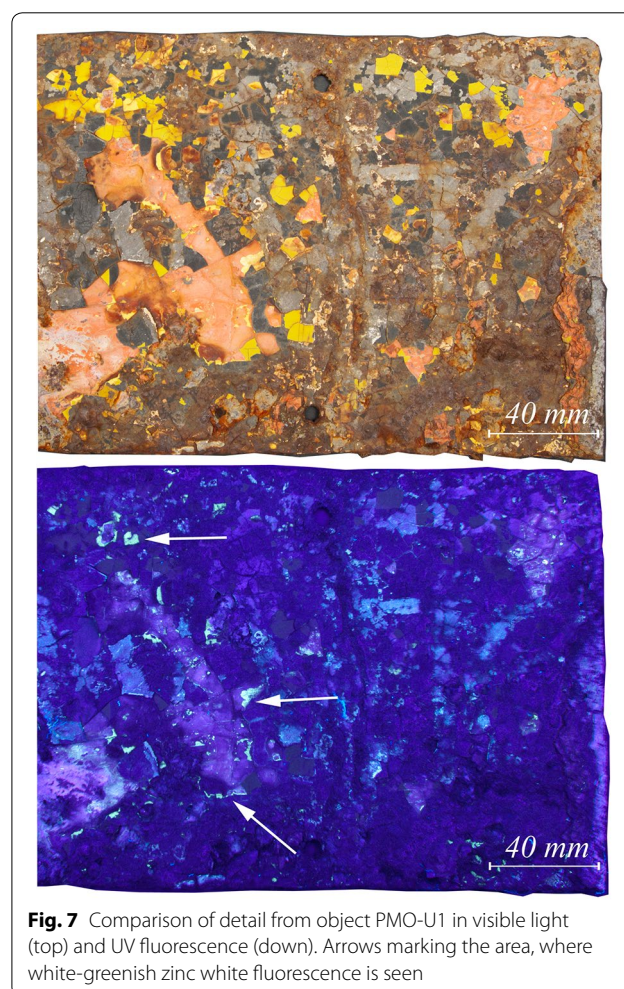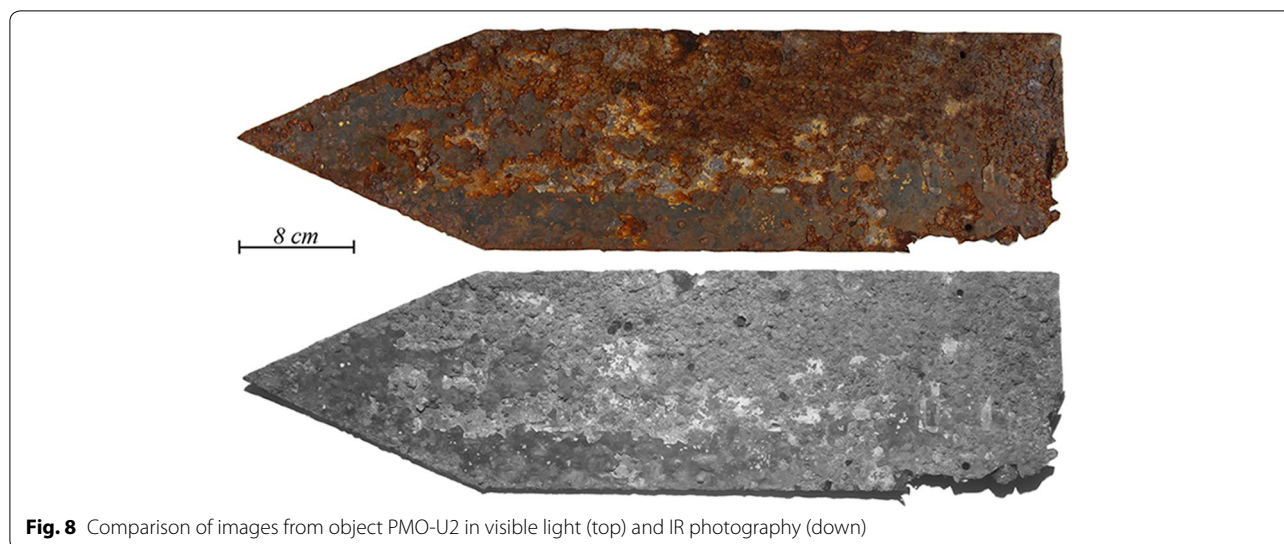

Fig. 7 Comparison of detail from object PMO-U1 in visible light (top) and UV fluorescence (down). Arrows marking the area, where white-greenish zinc white fluorescence is seen

Fig. 8 Comparison of images from object PMO-U2 in visible light (top) and IR photography (down)

We documented several delamination phenomena according to the stratigraphic evaluation of the paint sequences. They consisted of exfoliation between layers and losses of paint due to volume growth of the iron substrate induced by corrosion. This finding describes a common but nevertheless eminent problem of conservation science. A damage of paint causes loss of information which highlights the need for proper consolidation studies.

With elemental analysis inorganic pigments as titanium white, zinc white and several mineral extenders were detected. We identified synthetic organic materials, e.g. alkyds, cellulose nitrate or PY1 pigment (monoazo yellow) using instrumental analysis on a molecular level. The development and application of synthetic organic materials played a key role in the rise of the German *"Interessengemeinschaft Farben AG"* (I.G. Farben) during World War II. When this company built a synthesis plant next to the concentration camp Auschwitz III–Monowitz, it was explicitly planned to introduce a "binder on a synthetic base" in the so-called *"Lackplan"* (lacquer plan) from 1941 [51] in addition to the better known synthetic rubber (Buna) and fuels. The presented results indicate the availability of these materials for objects made in slave labour.

Our study could not find clear evidence for the presumed inscription. Future investigation could help to solve the issue e.g. by using spectral imaging in conjunction with image processing tools e.g. principal component analysis (PCA) [52] or spectral correlation mapping (SCM) [53]. In conjunction with the identified materials, SCM could provide more information about the spatial distribution of the pigments. Invasive micro-sampling is always destructive for cultural heritage objects and especially for objects made from painted or coated iron-containing substrates, because defects of the coating can provoke further corrosive mechanisms [54, 55]. Therefore, we reduced to a minimum in our study. Future research should additionally include complementary, non-destructive methods such as optical coherence tomography (OCT) [56, 57], macroscopic reflection mode FTIR (MA-rFTIR) [58] or multiphoton excitation fluorescence (MPEF) [59] to confirm and expand results concerning paint and corrosion layers.

Authors' contributions
GP conception of the project, acquisition and preparation of micro-samples, acquisition and interpretation of data; writing the article. MS designing and supervising the research work; drafting the article and final approval of the version to be published. WV supervising the acquisition and interpretation of FTIR data. BP designing and supervising the SEM–EDS data acquisition, contribution to the revision of this article. AJ contributing to the writing of this article concerning the historical background of the objects. All authors read and approved the final manuscript.

Availability of data and materials
Not applicable.

Pöllnitz *et al. Herit Sci*   (2019) 7:98

Page 11 of 12

Author details
[1] Institute of Science and Technology in Art, Academy of Fine Arts Vienna, Schillerplatz 3, 1010 Vienna, Austria. [2] Department of Archaeometry, Institute of Art and Technology, University of Applied Arts Vienna, Salzgries 14, 1010 Vienna, Austria. [3] Preservation Department, Auschwitz-Birkenau State Museum, ul. Wieźniów Oświęcimia 20, 32-603 Oświęcim, Poland.

References
1. Dębski J. Schilder und Tafeln - Beiträge zur Geschichte des KL Auschwitz. Hefte von Auschwitz. 2000;21:165–219.
2. Schulte JE. Rüstungsunternehmen oder Handwerksbetrieb? Das KZ-Häftlinge ausbeutende SS-Unternehmen "Deutsche Ausrüstungswerke GmbH." In: Herbert U, Orth K, Dieckmann C, editors. Die nationalsozialistischen Konzentrationslager: Entwicklung und Struktur. Wallstein Verlag; 1998. p. 558–83.
3. Świebocka T, Webber J, Wilsack C. Auschwitz: a history in photographs. Auschwitz-Birkenau State Museum O, editor. Indiana: University Press; 1993. 295 p.
4. Price B, Pretzel B, Carlson J, Ehrmann K: Promoting global access to the infrared and raman users group spectral database. In: Picollo M, editor. The sixth Infrared and Raman useres group conference (IRUG6), 293–142004, Florence/Italy. 2004. p. 17–25.
5. Schäning A, Schreiner M, Jembrih-Simbuerger D. Identification and classification of synthetic organic pigments of a collection of the 19th and 20th century by FTIR. In: The sixth Infrared and Raman users group Conference (IRUG6), 293–142004, Florence: Italy. 2004. p. 302–5.
6. Hummel DO. IR Hummel industrial polymers. CD-ROM. Vol 1–3. Hoboken: Wiley VCH; 2000.
7. Learner TJS. Tate organic pigment archive, unpublished FTIR reference spectra. London: Tate Gallery; 2003.
8. Scott D. Metallography and microstructure of ancient and historic metals. Averkieff I, editor. Los Angeles: Getty Conservation Institute; 1991.
9. Rössel T. Korrosionsschutz durch Bleimennige-Grundanstriche. Werkst Korros. 1969;20(10):854–60.
10. Lincke G, Mahn W. Warum wirkt Mennige auf Stahl korrosionsschützend, wenn Stahl noch Restrost an der Oberfläche enthält? defazet Dtsch Farben- Zeitschrift. 1974;28(1):423–4.
11. Forsgren A. Corrosion control through organic coatings. Taylor & Francis; 2006.
12. Appleby AJ, Mayne JEO. The relative protection afforded by red lead dispersed in linseed oil, tung oil, oiticica oil and a long oil alkyd varnish. J Oil Colour Chem Assoc. 1976;59(2):69–71.
13. Plater MJ, De Silva B, Gelbrich T, Hursthouse MB, Higgitt CL, Saunders DR. The characterisation of lead fatty acid soaps in "protrusions" in aged traditional oil paint. Polyhedron. 2003;22(24):3171–9.
14. Mayne JEO, Ramshaw EH. Autoxidation of the lead soaps of the linseed oil fatty acids. J Appl Chem. 1963;13(12):553–60.
15. Mayne JEO. Mechanisms of protection by paints. In: Cottis RA, editor. Shreir's corrosion 4th ed, Vol 4, Part III. Elsevier; 2010. p. 2666–77.
16. Evans UR. The corrosion and oxidation of metals: scientific principles and practical applications. London: Edward Arnold Publishers; 1960.
17. Eastaugh N, Walsh V, Chaplin T, Siddall R. Pigment compendium. London: Taylor and Francis; 2008.
18. Monico L, Van Der Snickt G, Janssens K, De Nolf W, Miliani C, Verbeeck J, et al. Degradation process of lead chromate in paintings by Vincent van Gogh studied by means of synchrotron X-ray spectromicroscopy and related methods. 2. Original paint layer samples. Anal Chem. 2010;83(4):1224–31.
19. Learner TJS. Analysis of modern paints. Los Angeles: Getty Publications; 2004.
20. Bussiere PO, Gardette JL, Therias S. Photodegradation of celluloid used in museum artifacts. Polym Degrad Stab. Elsevier Ltd. 2014;107:246–54.
21. Berthumeyrie S, Collin S, Bussiere PO, Therias S. Photooxidation of cellulose nitrate: new insights into degradation mechanisms. J Hazard Mater. 2014;272(2):137–47.
22. Shashoua Y, Bradley SM, Daniels VD. Degradation of cellulose nitrate adhesive. Stud Conserv. 1992;37(2):113–9.
23. Schweitzer PA. Paint and coatings: applications and corrosion resistance. New York City: Taylor & Francis; 2006.
24. Selwyn L. Metals and corrosion. A Handbook for the Conservation Professional. Ottawa: Canadian Conservation Institute; 2004.
25. Pintus V, Wei S, Schreiner M. Accelerated UV ageing studies of acrylic, alkyd, and polyvinyl acetate paints: Influence of inorganic pigments. Microchem J. 2016;124:949–61.
26. Rivenc R. Made in Los Angeles: materials, processes, and the birth of West Coast minimalism. Los Angeles: Getty Publications; 2016.
27. Kühn H, Curran M. Chrome yellow and other chromate Pigments. In: Feller RF, editor. Artists' pigments a handbook of their history and characteristics, vol. 1. London: Archetype Publications; 1985. p. 187–218.
28. Koleske J, editor. Paint and Coating Testing Manual. 14th ed. Philadelphia: ASTM Publishing; 1995.
29. Cornell RM, Schwertmann U. Iron Oxides: Structure, Properties, Reactions, Occurences and Uses. 2nd ed. Weinheim: Wiley VCH; 2003. p. 3–527.
30. Schwertmann U, Cornell RM. Iron oxides in the laboratory. Preparation and characterization. 2nd ed. Weinheim: Wiley VCH; 2000.
31. Miliani C, Rosi F, Burnstock A, Brunetti BG, Sgamellotti A. Non-invasive in situ investigations versus micro-sampling: a comparative study on a renoirs painting. Appl Phys A Mater Sci Process. 2007;89(4):849–56.
32. Vila A, Ferrer N, García JF. Chemical composition of contemporary black printing inks based on infrared spectroscopy: basic information for the characterization and discrimination of artistic prints. Anal Chim Acta. 2007;591(1):97–105.
33. Tomasini E, Siracusano G, Maier MS. Spectroscopic, morphological and chemical characterization of historic pigments based on carbon. Paths for the identification of an artistic pigment. Microchem J. 2012;102:28–37.
34. Daveri A, Malagodi M, Vagnini M. The bone black pigment identification by noninvasive, in situ infrared reflection spectroscopy. J Anal Methods Chem. 2018;2018:1–8.
35. Ren F, Ding Y, Leng Y. Infrared spectroscopic characterization of carbonated apatite: a combined experimental and computational study. J Biomed Mater Res Part A. 2014;102(2):496–505.
36. Derrick MR, Stulik D, Landry JM. Infrared spectroscopy in conservation science. Los Angeles: Getty Publications; 1999.
37. Infrared and Raman Users Group. http://www.irug.org/. 2017.
38. Miliani C, Sgamellotti A, Kahrim K, Brunetti BG, Aldrovandi A, van Bommel R, et al. MOLAB, a mobile facility suitable for non-invasive in situ investigations of early and contemporary paintings: case study-Victory Boogie Woogie (1942–1944) by Piet Mondrian. In: ICOM Committee for Conservation 15th Triennial Conference, New Delhi: 22–26 September 2008: Preprints. New Delhi: Allied Publishers; 2008.
39. Kühn H. Zinc White. In: Feller RF, editor. Artists' pigments a handbook of their history and characteristics, vol. 1. London: Archetype Publications; 1986. p. 169–86.
40. Wallinder IO, He W, Augustsson PE, Leygraf C. Characterization of black rust staining of unpassivated 55% Al–Zn alloy coatings. Effect of temperature, pH and wet storage. Corros Sci. 1999;41(12):2229–49.
41. Schmid EV. The use of micaceous iron oxide in longterm-corrosion protection. Pigment Resin Technol. 1986;15(1):4–7.
42. Eastaugh N, Walsh V, Chaplin T, Siddall R. Pigment compendium. Butterworth-Heinemann: A dictionary and optical microscopy of historical pigments; 2008.
43. de Keijzer M. The history of modern synthetic inorganic and organic artists' pigments. Contributions to conservation: research in conservation at the Netherlands Institute for Cultural Heritage (ICN Instituut Collectie Nederland). ICN Instituut Collectie Nederland; 2002. p. 42–54.
44. Herbst W, Hunger K, Wilker G, Ohleier H, Winter R. Industrial Organic Pigments. 3rd ed. Weinheim: Wiley VCH; 2004.
45. Lomax SQ, Schilling MR, Learner TJS. The identification of synthetic organic pigments by FTIR and DTMS. In: Learner TJS, Smithen P, Krueger JW, Schilling MR, editors. Modern paints uncovered tate modern, London

May 16–19, 2006. Los Angeles: Getty Conservation Institute; 2006. p. 105–17.

46. Kittel H. Pigmente. Herstellung, Eigenschaften, Anwendung. 3., völlig. Stuttgart: Wissenschaftliche Verlagsgesellschaft mbH; 1960. p 505.

47. Lauridsen CB, Sanyova J, Simonsen KP. Analytical study of modern paint layers on metal knight shields: the use and effect of titanium white. Spectrochim Acta A. 2014;124:638–45.

48. Titanium Laver M, Whites Dioxide. In: Fitzhugh EW, Feller R, Ashok R, editors. Artists' pigments: a handbook of their history and characteristics, vol. 3. Oxford: Oxford University Press; 1997. p. 295–355.

49. Carlyle L, Boon JJ, Haswell R, Stols-Witlox M. Historically accurate ground reconstructions for oil paintings. In: Townsend JH, Doherty T, Heydenreich G, Ridge J, editors. Preparation for painting: the artist's choice and its consequences. London: Archetype Publications; 2008. p. 110–22.

50. Cosentino A. Effects of different binders on technical photography and infrared reflectography of 54 historical pigments. Int J Conserv Sci. 2015;6(3):287–98.

51. Goethe-Universität Frankfurt am Main. I.G. Auschwitz, 1. Baubesprechung am 24.3.1941 in Ludwigshafen/Rh., 31.3.1941, NI-11115. Archiv des Fritz Bauer Instituts, Nürnberger Nachfolgeprozess Fall VI, ADB 72 (d), Bl. 158–179, hier Bl. 160. cited on: http://www.wollheim-memorial.de, Access 01.11. 2019.

52. Baronti S, Casini A, Lotti F, Porcinai S. Segmentation of multispectral images of works of art through principal component analysis. Lect Notes Comput Sci. 1997;1310:14–21.

53. Deborah H, George S, Hardeberg JY. Pigment mapping of the scream (1893) based on hyperspectral imaging. Lect Notes Comput Sci. 1893;2014(8509):247–56.

54. Stratmann M. Corrosion stability of polymer-coated metals—New concepts based on fundamental understanding. Corrosion. 2005;61(12):1115–26.

55. Posner R, Ozcan O, Grundmeier G. Water and Ions at Polymer/Metal Interfaces. In: da Silva LFM, Sato C, editors. Design of adhesive joints under humid conditions advanced structured materials 25. 2013. p. 21–52.

56. Targowski P, Iwanicka M. Optical coherence tomography: its role in the non-invasive structural examination and conservation of cultural heritage objects—A review. Appl Phys A Mater Sci Process. 2012;106(2):265–77.

57. Targowski P, Pronobis-Gajdzis M, Surmak A, Iwanicka M, Kaszewska EA, Sylwestrzak M. The application of macro-X-ray fluorescence and optical coherence tomography for examination of parchment manuscripts. Stud Conserv. 2015;60(sup1):S167–77.

58. Legrand S, Ricciardi P, Nodari L, Janssens K. Non-invasive analysis of a 15th century illuminated manuscript fragment: point-based vs imaging spectroscopy. Microchem J. 2018;138:162–72.

59. Faraldi F, Tserevelakis G, Filippidis G, Ingo G, Riccucci C, Fotakis C. Multi photon excitation fluorescence imaging microscopy for the precise characterization of corrosion layers in silver-based artifacts. Appl Phys A. 2013;111:177–81.

Publisher's Note

Springer Nature remains neutral with regard to jurisdictional claims in published maps and institutional affiliations.